Neutron skin thickness of ^{208}Pb determined from the reaction cross section for proton scattering

Shingo Tagami,[1] Tomotsugu Wakasa,[1] Jun Matsui,[1] Masanobu Yahiro,[1,*] and Maya Takechi[2]
[1]*Department of Physics, Kyushu University, Fukuoka 819-0395, Japan*
[2]*Niigata University, Niigata 950-2181, Japan*

(Received 9 March 2021; revised 29 April 2021; accepted 21 July 2021; published 9 August 2021)

Background: The reaction cross section σ_R is useful to determine the neutron radius R_n as well as the matter radius R_m. The chiral (Kyushu) g-matrix folding model for ^{12}C scattering on ^{9}Be, ^{12}C, ^{27}Al targets was tested in the incident energy range of $30 \lesssim E_{\rm in} \lesssim 400$ MeV, and it is found that the model reliably reproduces the σ_R in $30 \lesssim E_{\rm in} \lesssim 100$ MeV and $250 \lesssim E_{\rm in} \lesssim 400$ MeV.
Purpose: Our aim is to determine $r_{\rm skin}^{208}$(EXP) from $\sigma_{\rm R}$(EXP) for $p + {}^{208}$Pb scattering in $30 \leqslant E_{\rm lab} \leqslant 100$ MeV.
Methods: Our model is the Kyushu g-matrix folding model with the densities calculated with Gongny-D1S HFB (GHFB) with the angular momentum projection (AMP).
Results: The Kyushu g-matrix folding model with the GHFB+AMP densities underestimates $\sigma_{\rm R}$ in $30 \leqslant E_{\rm in} \leqslant 100$ MeV only by a factor of 0.97. Since the proton radius R_p calculated with GHFB+AMP agrees with the precise experimental data of 5.444 fm, the small deviation of the theoretical result from the data on σ_R allows us to scale the GHFB+AMP neutron density so as to reproduce the σ_R data. In $E_{\rm in} = 30$–100 MeV, the experimental σ_R data can be reproduced by assuming the neutron radius of ^{208}Pb as $R_n = 5.722 \pm 0.035$ fm.
Conclusion: The present result $R_{\rm skin} = 0.278 \pm 0.035$ fm is in good agreement with the recent PREX-II result of $r_{\rm skin} = 0.283 \pm 0.071$ fm.

DOI: 10.1103/PhysRevC.104.024606

I. INTRODUCTION

Horowitz *et al.* [1] proposed a direct measurement for neutron skin $R_{\rm skin} = R_n - R_p$, where $R_n \equiv \langle r_n^2\rangle^{1/2}$ and $R_p \equiv \langle r_p^2\rangle^{1/2}$ are the root-mean-square (rms) radii of point neutrons and protons, respectively. The measurement consists of parity-violating (PV) and elastic electron scattering. The neutron radius R_n is determined from the former experiment, whereas the proton radius R_p is from the latter.

Very recently, by combining the original lead radius experiment (PREX) result [2,3] with the updated PREX-II result, the PREX collaboration reported the following value [4]:

$$R_{\rm skin}^{PV} = 0.283 \pm 0.071\,{\rm fm}, \tag{1}$$

where the quoted uncertainty represents a 1σ error and has been greatly reduced from the original value of ± 0.177 fm (quadratic sum of experimental and model uncertainties) [3]. The $R_{\rm skin}^{PV}$ value is most reliable at the present stage, and provides crucial tests for the equation of state (EoS) of nuclear matter [5–9] as well as nuclear structure models. For example, Reed *et al.* [10] report a value of the slope parameter L of the EoS and examine the impact of such a stiff symmetry energy on some critical neutron-star observables. It should be noted that the $R_{\rm skin}^{PV}$ value is considerably larger than other experimental values that are significantly model dependent [11–14]. As an exceptional case, a nonlocal dispersive-optical-model (DOM) analysis of ^{208}Pb deduces $r_{\rm skin}^{\rm DOM} = 0.25 \pm 0.05$ fm [15]. It is the aim of this paper to present the $R_{\rm skin}$ value with a similar precision of $R_{\rm skin}^{PV}$ by analyzing the reaction cross section σ_R for $p + {}^{208}$Pb.

The reaction cross section σ_R is a powerful tool to determine matter radius R_m. One can evaluate $R_{\rm skin}$ and R_n by using the R_m and the R_p [16] determined by the electron scattering. The g-matrix folding model is a standard way of deriving microscopic optical potential for not only proton scattering but also nucleus-nucleus scattering [17–27]. Applying the folding model with the Melbourne g matrix [20] for interaction cross sections $\sigma_{\rm I}$ for Ne isotopes and $\sigma_{\rm R}$ for Mg isotopes, we discovered that ^{31}Ne is a halo nucleus with large deformation [27], and deduced the matter radii $r_{\rm m}$ for Ne isotopes [28] and for Mg isotopes [29]. The folding potential is nonlocal, but is localized with the method of Ref. [17]. The validity is shown in Ref. [30]. For proton scattering, the localized version of g-matrix folding model [31] yields the same results as the full folding g-matrix folding model of Ref. [20], as shown by comparing the results of Ref. [31] with those of Ref. [20].

Recently, Kohno [32] calculated the g matrix for the symmetric nuclear matter, using the Brueckner-Hartree-Fock method with chiral fourth-order (N^{3}LO) nucleon-nucleon (NN) forces (2NFs) and third-order (NNLO) three-nucleon forces (3NFs). He set $c_D = -2.5$ and $c_E = 0.25$ so that the energy per nucleon can become minimum at $\rho = \rho_0$; see Fig. 1 for c_D and c_E. Toyokawa *et al.* [25] localized the nonlocal chiral g matrix into three-range Gaussian forms. using the localization method proposed by the Melbourne group [20,33,34]. The resulting local g matrix is called Kyushu g matrix.

The Kyushu g-matrix folding model is successful in reproducing $\sigma_{\rm R}$ and differential cross sections $d\sigma/d\Omega$ for ^{4}He

*orion093g@gmail.com

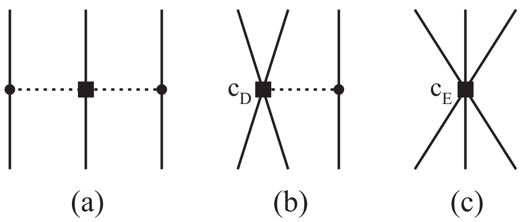

FIG. 1. 3*N*Fs in NNLO. Diagram (a) corresponds to the Fujita-Miyazawa 2π exchange 3*NF* [35], and diagrams (b) and (c) correspond to 1π exchange and contact 3*N*Fs. The solid and dashed lines denote nucleon and pion propagations, respectively, and filled circles and squares stand for vertices. The strength of the filled-square vertex is often called c_D in diagram (b) and c_E in diagram (c).

scattering in $E_{\rm in} = 30$–200 MeV/nucleon [25]. The success is true for proton scattering at $E_{\rm in} = 65$ MeV [23]. Lately, we predicted neutron skin $r_{\rm skin}$ and proton, neutron, matter radii, R_p, R_n, R_m from interaction cross sections $\sigma_{\rm I}$ ($\approx \sigma_{\rm R}$) for $^{42-51}$Ca + ^{12}C scattering at $E_{\rm in} = 280$ MeV/nucleon, using the Kyushu *g*-matrix folding model with the densities calculated with Gongny-D1S HFB (GHFB) with and without the angular momentum projection (AMP) [26].

In Ref. [26], we tested the Kyushu *g*-matrix folding model for ^{12}C scattering on ^{9}Be, ^{12}C, ^{27}Al targets in $30 \lesssim E_{\rm in} \lesssim 400$ MeV, comparing the theoretical $\sigma_{\rm R}$ with the experimental data [36]. We found that the Kyushu *g*-matrix folding model is reliable for $\sigma_{\rm R}$ in $30 \lesssim E_{\rm in} \lesssim 100$ MeV and $250 \lesssim E_{\rm in} \lesssim 400$ MeV. This indicates that the Kyushu *g*-matrix folding model is applicable in $30 \leqslant E_{\rm lab} \leqslant 100$ MeV, although the data on $p + {}^{208}$Pb scattering are available in $21 \leqslant E_{\rm lab} \leqslant 180$ MeV.

In this paper, we present the determination of $R_{\rm skin}^{\rm GHFB}$ from the measured σ_R for $p + {}^{208}$Pb scattering in $30 \leqslant E_{\rm in} \leqslant 100$ MeV [37–39], using the Kyushu *g*-matrix folding model with the GHFB+AMP densities. As mentioned above, the Kyushu *g*-matrix folding model is applicable in $30 \leqslant E_{\rm in} \leqslant 100$ MeV, although the data on $p + {}^{208}$Pb scattering are available in $21 \leqslant E_{\rm in} \leqslant 180$ MeV. In Sec. II, we briefly describe our model. Section III presents the results and a comparison with $R_{\rm skin}^{PV}$, and discussion follows. Finally, Sec. IV is devoted to a summary.

II. MODEL

Our model is the Kyushu *g*-matrix folding model [25] with the densities calculated with GHFB+AMP [26]. In Ref. [25], the Kyushu *g* matrix is constructed from chiral interaction with the cutoff $\Lambda = 550$ MeV. The model was tested for ^{12}C scattering on ^{9}Be, ^{12}C, and ^{27}Al targets in $30 \lesssim E_{\rm in} \lesssim 400$ MeV. It is found that the Kyushu *g*-matrix folding model is good in $30 \lesssim E_{\rm in} \lesssim 100$ MeV and $250 \lesssim E_{\rm in} \lesssim 400$ MeV [26].

The brief formulation of the folding model itself is shown below. For nucleon-nucleus scattering, the potential is composed of the direct and exchange parts, $U^{\rm DR}$ and $U^{\rm EX}$ [29]:

$$U^{\rm DR}(\boldsymbol{R}) = \sum_{\mu,\nu} \int \rho_{\rm T}^{\nu}(\boldsymbol{r}_{\rm T}) g_{\mu\nu}^{\rm DR}(s;\rho_{\mu\nu}) d\boldsymbol{r}_{\rm T}, \tag{2a}$$

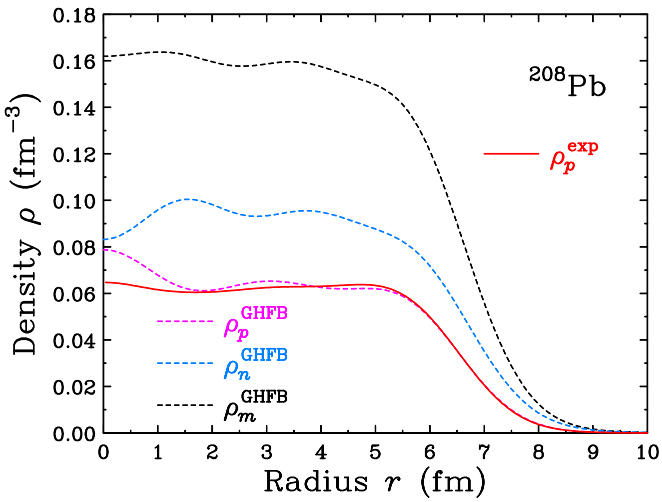

FIG. 2. r dependence of densities, $\rho_p(r)$, $\rho_n(r)$, $\rho_m(r)$, for ^{208}Pb calculated with GHFB+AMP. Three dashed lines from the bottom to the top denote $\rho_p(r)$, $\rho_n(r)$, $\rho_m(r)$, respectively. The experimental point-proton (unfolded) density ρ_p is taken from Refs. [40,41].

$$U^{\rm EX}(\boldsymbol{R}) = \sum_{\mu,\nu} \int \rho_{\rm T}^{\nu}(\boldsymbol{r}_{\rm T}, \boldsymbol{r}_{\rm T} + \boldsymbol{s}) \times g_{\mu\nu}^{\rm EX}(s;\rho_{\mu\nu}) \exp[-i\boldsymbol{K}(\boldsymbol{R})\cdot \boldsymbol{s}/M] d\boldsymbol{r}_{\rm T}, \tag{2b}$$

where $\boldsymbol{R}$ is the relative coordinate between a projectile (P) and a target (T), $\boldsymbol{s} = -\boldsymbol{r}_{\rm T} + \boldsymbol{R}$, and $\boldsymbol{r}_{\rm T}$ is the coordinate of the interacting nucleon from T. Each of μ and ν denotes the z component of isospin; 1/2 means neutron and $-1/2$ does proton. The nonlocal $U^{\rm EX}$ has been localized in Eq. (2b) with the local semi-classical approximation [17], where $K(R)$ is the local momentum between P and T, and $M = A/(1 + A)$ for the target mass number A; see Ref. [30] for the validity of the localization. The direct and exchange parts, $g_{\mu\nu}^{\rm DR}$ and $g_{\mu\nu}^{\rm EX}$, of the g matrix depend on the local density

$$\rho_{\mu\nu} = \rho_{\rm T}^{\nu}(\boldsymbol{r}_{\rm T} + \boldsymbol{s}/2), \tag{3}$$

at the midpoint of the interacting nucleon pair; see Ref. [28] for the explicit forms of $g_{\mu\nu}^{\rm DR}$ and $g_{\mu\nu}^{\rm EX}$.

The relative wave function ψ is decomposed into partial waves χ_L, each with different orbital angular momentum L. The elastic S-matrix elements S_L are obtained from the asymptotic form of the χ_L. The total reaction cross section $\sigma_{\rm R}$ is calculable from the S_L as

$$\sigma_{\rm R} = \frac{\pi}{K^2} \sum_L (2L+1)(1 - |S_L|^2). \tag{4}$$

The proton and neutron densities, $\rho_p(r)$ and $\rho_n(r)$, are calculated with GHFB+AMP. As a way of taking the center-of-mass correction to the densities, we use the method of Ref. [28], since the procedure is quite simple.

III. RESULTS

Figure 2 shows the proton $\rho_p^{\rm GHFB}$, neutron $\rho_n^{\rm GHFB}$, and matter $\rho_m^{\rm GHFB} \equiv \rho_p^{\rm GHFB} + \rho_n^{\rm GHFB}$ densities as a function of r. The experimental point-proton distribution extracted from the

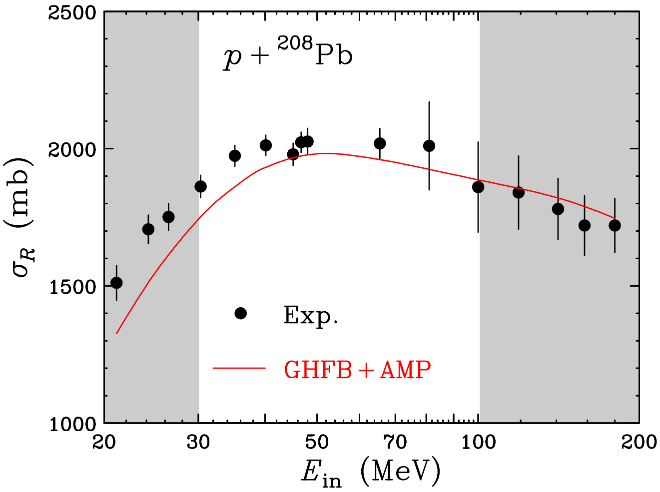

FIG. 3. $E_{\rm in}$ dependence of reaction cross sections $\sigma_{\rm R}$ for $p + {}^{208}$Pb scattering. The solid line stands for the results of the Kyushu g-matrix folding model with GHFB+AMP densities. The data are taken from Refs. [37–39].

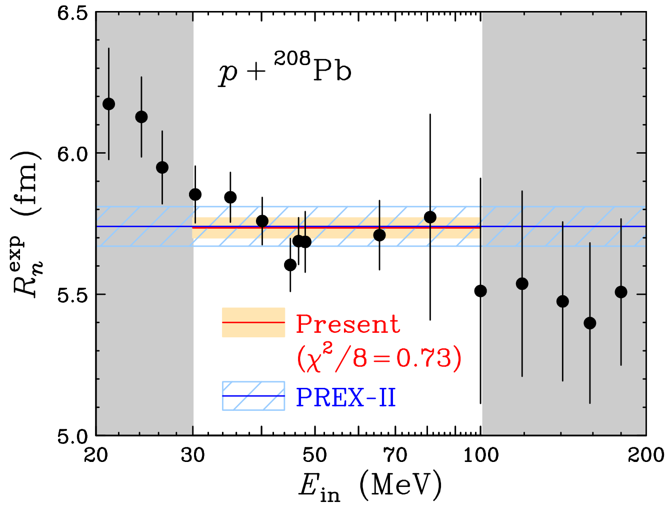

FIG. 4. Neutron radius $R_n^{\rm exp}$ of ^{208}Pb deduced from the $p + {}^{208}$Pb reaction cross section and the theoretical Kyushu g-matrix folding model calculations as a function of infident energy $E_{\rm in}$.

electron scattering data is also shown. The theoretical proton distribution $\rho_p^{\rm GHFB}$ reproduces the experimental $\rho_p^{\rm exp}$ reasonably well.

The Kyushu g-matrix folding model with the GHFB+AMP densities underestimates the σ_R data in $30 \leqslant E_{\rm in} \leqslant 100$ MeV only by a factor of 0.97, as shown in Fig. 3. The proton radius $R_p^{\rm GHFB} = 5.444$ fm calculated with GHFB+AMP agrees with the experimental value of $R_p^{\rm exp} = 5.444$ fm [42]. Because of $\sigma_R \propto R_m^2$, the observed discrepancy of σ_R is attributed to the underestimation of $\rho_m^{\rm GHFB}$ originating from the underestimation of $\rho_n^{\rm GHFB}$. Small deviation makes it possible to scale the GHFB+AMP densities for the neutron density so as to reproduce $\sigma_R^{\rm exp}$ in $E_{\rm in} = 30$–100 MeV. The result of the scaling is $R_n^{\rm exp} = 5.722 \pm 0.035$ fm leading to

$$R_{\rm skin}^{\rm exp} = 0.278 \pm 0.035 \,{\rm fm}. \tag{5}$$

This result is consistent with $R_{\rm skin}^{PV} = 0.283 \pm 0.071$ fm.

Now we show a simple derivation of $R_n^{\rm exp}$ in the limit of $K^{\rm exp} = K^{\rm th}$. The experimental and theoretical (GHFB+AMP) reaction cross sections, $\sigma_R^{\rm exp}$ and $\sigma_R^{\rm th}$, can be expressed as

$$\sigma_R^{\rm exp} = K^{\rm exp}\left[\left(R_p^{\rm exp}\right)^2 \frac{Z}{A} + \left(R_n^{\rm exp}\right)^2 \frac{N}{A}\right], \tag{6a}$$

$$\sigma_R^{\rm th} = K^{\rm th}\left[\left(R_p^{\rm th}\right)^2 \frac{Z}{A} + \left(R_n^{\rm th}\right)^2 \frac{N}{A}\right], \tag{6b}$$

where Z, N, and A are proton, neutron, and atomic numbers of ^{208}Pb, respectively, and K is a proportional coefficient between σ_R and $R_m^2 = R_p^2(Z/A) + R_n^2(N/A)$. By using $K^{\rm exp} = K^{\rm th}$ and $R_p^{\rm exp} = R_p^{\rm th}$, the experimental neutron radius $R_n^{\rm exp}$ can be deduced as

$$R_n^{\rm exp} = \sqrt{\frac{Z\left(R_p^{\rm exp}\right)^2 + N\left(R_n^{\rm th}\right)^2}{N\sigma_R^{\rm th}}\sigma_R^{\rm exp} - \left(\sigma_p^{\rm exp}\right)^2 \frac{Z}{N}}, \tag{7}$$

from the experimental $\sigma_R^{\rm exp}$ and $R_p^{\rm exp}$ data and the theoretical $R_n^{\rm th}$ in GHFB+AMP.

Figure 4 shows the $R_n^{\rm exp}$ results as a function of incident energy $E_{\rm in}$. The deduced $R_n^{\rm exp}$ values are almost independent of $E_{\rm in}$ in the region of $E_{\rm in} = 30$–100 MeV where the present folding model is reliable [26]. By combining the eight data in this energy region, the neutron radius of ^{208}Pb becomes $\overline{R}_n^{\rm exp} = 5.735 \pm 0.035$ fm as shown by the filled band in Fig. 4. This result shows that the neutron skin thickness of ^{208}Pb is $R_{\rm skin}^{\rm exp} = 0.291 \pm 0.035$ fm with $R_p^{\rm exp} = 5.444$ fm [42]. The limit of $K^{\rm exp} = K_R^{\rm th}$ is thus good, since $R_{\rm skin}^{\rm exp} = 0.291 \pm 0.035$ fm is close to Eq. (5). Equation (7) is quite useful when $\sigma_R^{\rm exp} \approx \sigma_R^{\rm th}$ and $R_p^{\rm exp} \approx R_p^{\rm th}$.

IV. SUMMARY

The proton radius R_p calculated with GHFB+AMP agrees with the precise experimental data of 5.444 fm. In $30 \leqslant E_{\rm in} \leqslant 100$ MeV, we can obtain $r_{\rm n}^{\rm exp}$ from $\sigma_{\rm R}^{\rm exp}$ by scaling the GHFB+AMP neutron density so as to reproduce $\sigma_{\rm R}^{\rm exp}$ for each $E_{\rm in}$, and take the weighted mean and its error for the resulting $r_{\rm n}^{\rm exp}$. From the resulting $R_n^{\rm exp} = 5.722 \pm 0.035$ fm and $r_{\rm p}^{\rm exp} = 5.444$ fm, we can get $R_{\rm skin}^{\rm exp} = 0.278 \pm 0.035$ fm. In conclusion, our result $R_{\rm skin}^{\rm exp} = 0.278 \pm 0.035$ fm is consistent with a new result $r_{\rm skin}^{208}$(PREX II) $= 0.283 \pm 0.071$ fm of PREX-II.

ACKNOWLEDGMENT

We would like to thank Dr. Toyokawa for providing his code.

[1] C. J. Horowitz, S. J. Pollock, P. A. Souder, and R. Michaels, Phys. Rev. C **63**, 025501 (2001).
[2] S. Abrahamyan, Z. Ahmed, H. Albataineh, K. Aniol, D. S. Armstrong, W. Armstrong, T. Averett, B. Babineau, A. Barbieri, V. Bellini *et al.* (PREX Collaboration), Phys. Rev. Lett. **108**, 112502 (2012).
[3] C. J. Horowitz, Z. Ahmed, C.-M. Jen, A. Rakhman, P. A. Souder, M. M. Dalton, N. Liyanage, K. D. Paschke, K. Saenboonruang, R. Silwal, G. B. Franklin, M. Friend, B. Quinn, K. S. Kumar, D. McNulty, L. Mercado, S. Riordan, J. Wexler, R. W. Michaels, and G. M. Urciuoli, Phys. Rev. C **85**, 032501(R) (2012).
[4] D. Adhikari, H. Albataineh, D. Androic, K. Aniol, D. S. Armstrong, T. Averett, S. Barcus, V. Bellini, R. S. Beminiwattha, J. F. Benesch *et al.* (PREX Collaboration), Phys. Rev. Lett. **126**, 172502 (2021).
[5] S. J. Novario, G. Hagen, G. R. Jansen, and T. Papenbrock, Phys. Rev. C **102**, 051303(R) (2020).
[6] H. Shen, F. Ji, J. Hu, and K. Sumiyoshi, Astrophys. J. **891**, 148 (2020).
[7] C. Horowitz, Ann. Phys. (Amsterdam) **411**, 167992 (2019).
[8] J.-B. Wei, J.-J. Lu, G. F. Burgio, Z.-H. Li, and H.-J. Schulze, Eur. Phys. J. A **56**, 63 (2020).
[9] M. Thiel, C. Sfienti, J. Piekarewicz, C. J. Horowitz, and M. Vanderhaeghen, J. Phys. G: Nucl. Part. Phys. **46**, 093003 (2019).
[10] B. T. Reed, F. J. Fattoyev, C. J. Horowitz, and J. Piekarewicz, Phys. Rev. Lett. **126**, 172503 (2021).
[11] A. Trzcińska, J. Jastrzębski, P. Lubiński, F. J. Hartmann, R. Schmidt, T. von Egidy, and B. Kłos, Phys. Rev. Lett. **87**, 082501 (2001).
[12] J. Zenihiro, H. Sakaguchi, T. Murakami, M. Yosoi, Y. Yasuda, S. Terashima, Y. Iwao *et al.*, Phys. Rev. C **82**, 044611 (2010).
[13] A. Tamii, I. Poltoratska, P. von Neumann-Cosel, Y. Fujita, T. Adachi, C. A. Bertulani, J. Carter *et al.*, Phys. Rev. Lett. **107**, 062502 (2011).
[14] C. M. Tarbert, D. P. Watts, D. I. Glazier, P. Aguar, J. Ahrens, J. R. M. Annand, H. J. Arends, R. Beck, V. Bekrenev, B. Boillat *et al.* (Crystal Ball at MAMI and A2 Collaboration), Phys. Rev. Lett. **112**, 242502 (2014).
[15] M. C. Atkinson, M. H. Mahzoon, M. A. Keim, B. A. Bordelon, C. D. Pruitt, R. J. Charity, and W. H. Dickhoff, Phys. Rev. C **101**, 044303 (2020).
[16] I. Angeli and K. Marinova, At. Data Nucl. Data Tables **99**, 69 (2013).
[17] F. Brieva and J. Rook, Nucl. Phys. A **291**, 299 (1977); **291**, 317 (1977); **297**, 206 (1978).
[18] G. Satchler and W. Love, Phys. Rep. **55**, 183 (1979); G. R. Satchler, *Direct Nuclear Reactions* (Oxford University Press, Oxford, 1983).
[19] N. Yamaguchi, S. Nagata, and T. Matsuda, Prog. Theor. Phys. **70**, 459 (1983); S. Nagata, M. Kamimura, and N. Yamaguchi, *ibid.* **73**, 512 (1985); N. Yamaguchi, S. Nagata, and J. Michiyama, *ibid.* **76**, 1289 (1986).
[20] K. Amos, P. J. Dortmans, H. V. von Geramb, S. Karataglidis, and J. Raynnal, in *Advances in Nuclear Physics*, edited by J. W. Negele and E. Vogt (Springer, Boston, 2000), pp. 276–536.
[21] T. Furumoto, Y. Sakuragi, and Y. Yamamoto, Phys. Rev. C **78**, 044610 (2008); **79**, 011601(R) (2009); **80**, 044614 (2009).
[22] K. Egashira, K. Minomo, M. Toyokawa, T. Matsumoto, and M. Yahiro, Phys. Rev. C **89**, 064611 (2014).
[23] M. Toyokawa, K. Minomo, M. Kohno, and M. Yahiro, J. Phys. G: Nucl. Part. Phys. **42**, 025104 (2014); **44**, 079502 (2017).
[24] M. Toyokawa, M. Yahiro, T. Matsumoto, K. Minomo, K. Ogata, and M. Kohno, Phys. Rev. C **92**, 024618 (2015); **96**, 059905(E) (2017).
[25] M. Toyokawa, M. Yahiro, T. Matsumoto, and M. Kohno, Prog. Theor. Exp. Phys. **2018**, 023D03 (2018).
[26] S. Tagami, M. Tanaka, M. Takechi, M. Fukuda, and M. Yahiro, Phys. Rev. C **101**, 014620 (2020).
[27] K. Minomo, T. Sumi, M. Kimura, K. Ogata, Y. R. Shimizu, and M. Yahiro, Phys. Rev. Lett. **108**, 052503 (2012).
[28] T. Sumi, K. Minomo, S. Tagami, M. Kimura, T. Matsumoto, K. Ogata, Y. R. Shimizu, and M. Yahiro, Phys. Rev. C **85**, 064613 (2012).
[29] S. Watanabe, K. Minomo, M. Shimada, S. Tagami, M. Kimura, M. Takechi, M. Fukuda, D. Nishimura, T. Suzuki, T. Matsumoto *et al.*, Phys. Rev. C **89**, 044610 (2014).
[30] K. Minomo, K. Ogata, M. Kohno, Y. R. Shimizu, and M. Yahiro, J. Phys. G: Nucl. Part. Phys. **37**, 085011 (2010).
[31] M. Toyokawa, K. Minomo, and M. Yahiro, Phys. Rev. C **88**, 054602 (2013).
[32] M. Kohno, Phys. Rev. C **88**, 064005 (2013); **96**, 059903(E) (2017).
[33] H. V. von Geramb, K. Amos, L. Berge, S. Bräutigam, H. Kohlhoff, and A. Ingemarsson, Phys. Rev. C **44**, 73 (1991).
[34] P. J. Dortmans and K. Amos, Phys. Rev. C **49**, 1309 (1994).
[35] J. Fujita and H. Miyazawa, Prog. Theor. Phys. **17**, 360 (1957); **17**, 366 (1957).
[36] M. Takechi, M. Fukuda, M. Mihara, K. Tanaka, T. Chinda, T. Matsumasa, M. Nishimoto, R. Matsumiya, Y. Nakashima, H. Matsubara, K. Matsuta, T. Minamisono, T. Ohtsubo, T. Izumikawa, S. Momota, T. Suzuki, T. Yamaguchi, R. Koyama, W. Shinozaki, M. Takahashi, A. Takizawa, T. Matsuyama, S. Nakajima, K. Kobayashi, M. Hosoi, T. Suda, M. Sasaki, S. Sato, M. Kanazawa, and A. Kitagawa, Phys. Rev. C **79**, 061601(R) (2009).
[37] R. F. Carlson, A. J. Cox, J. R. Nimmo, N. E. Davison, S. A. Elbakr, J. L. Horton, A. Houdayer, A. M. Sourkes, W. T. H. van Oers, and D. J. Margaziotis, Phys. Rev. C **12**, 1167 (1975).
[38] A. Ingemarsson, J. Nyberg, P. Renberg, O. Sundberg, R. Carlson, A. Auce, R. Johansson, G. Tibell, B. Clark, L. Kurth Kerr, and S. Hama, Nucl. Phys. A **653**, 341 (1999).
[39] A. Auce, A. Ingemarsson, R. Johansson, M. Lantz, G. Tibell, R. F. Carlson, M. J. Shachno, A. A. Cowley, G. C. Hillhouse, N. M. Jacobs *et al.*, Phys. Rev. C **71**, 064606 (2005).
[40] H. De Vries, C. De Jager, and C. De Vries, At. Data Nucl. Data Tables **36**, 495 (1987).
[41] H. Euteneuer, J. Friedrich, and N. Voegler, Nucl. Phys. A **298**, 452 (1978).
[42] A. B. Jones and B. A. Brown, Phys. Rev. C **90**, 067304 (2014).